Acta Crystallographica Section F
Structural Biology and Crystallization Communications
ISSN 1744-3091

Three crystal forms of the bifunctional enzyme proline utilization A (PutA) from *Bradyrhizobium japonicum*

Jonathan P. Schuermann,[a] Tommi A. White,[b] Dhiraj Srivastava,[a] Dale B. Karr[c] and John J. Tanner[a,b]*

[a]Department of Chemistry, University of Missouri-Columbia, Columbia, MO 65211, USA, [b]Department of Biochemistry, University of Missouri-Columbia, Columbia, MO 65211, USA, and [c]Structural Biology Core, University of Missouri-Columbia, Columbia, MO 65211, USA

Correspondence e-mail: tannerjj@missouri.edu

Received 22 August 2008
Accepted 5 September 2008

Proline utilization A proteins (PutAs) are large (1000–1300 residues) membrane-associated bifunctional flavoenzymes that catalyze the two-step oxidation of proline to glutamate by the sequential action of proline dehydrogenase and Δ^1-pyrroline-5-carboxylate dehydrogenase domains. Here, the first successful crystallization efforts for a PutA protein are described. Three crystal forms of PutA from *Bradyrhizobium japonicum* are reported: apparent tetragonal, hexagonal and centered monoclinic. The apparent tetragonal and hexagonal crystals were grown in the presence of PEG 3350 and sodium formate near pH 7. The apparent tetragonal form diffracted to 2.7 Å resolution and exhibited pseudo-merohedral twinning such that the true space group is $P2_12_12_1$ with four molecules in the asymmetric unit. The hexagonal form diffracted to 2.3 Å resolution and belonged to space group $P6_222$ with one molecule in the asymmetric unit. Centered monoclinic crystals were grown in ammonium sulfate, diffracted to 2.3 Å resolution and had two molecules in the asymmetric unit. Removing the histidine tag was important in order to obtain the *C*2 crystal form.

1. Introduction

All organisms catabolize proline by oxidizing it to glutamate in two enzymatic steps (Adams & Frank, 1980; Phang, 1985). In the first step, proline (**1** in Fig. 1) is oxidized to Δ^1-pyrroline-5-carboxylate (P5C; **2**) by the flavin-dependent enzyme proline dehydrogenase (PRODH; EC 1.5.99.8). P5C is then hydrolyzed nonenzymatically to glutamate semialdehyde (**3**), which is subsequently oxidized to glutamate (**4**) by the NAD^+-dependent enzyme P5C dehydrogenase (P5CDH; EC 1.5.1.12). The collective activities of PRODH and P5CDH result in the four-electron oxidation of proline to glutamate.

The arrangement of the genes encoding proline-catabolic enzymes differs from organism to organism. PRODH and P5CDH are separate enzymes encoded by distinct genes in eukaryotes and some bacteria, such as *Thermus thermophilus* (White *et al.*, 2007). In other bacteria, primarily Gram-negative species, PRODH and P5CDH are fused into a single polypeptide chain known as PutA (proline utilization A; Ratzkin & Roth, 1978; Menzel & Roth, 1981*a*; Brown & Wood, 1993; Surber & Maloy, 1998; Becker & Thomas, 2001; Vinod *et al.*, 2002; Zhu & Becker, 2003).

PutAs typically contain 1000–1300 amino-acid residues, with the PRODH domain located in the N-terminal half of the polypeptide chain and the P5CDH domain located in the C-terminal half. In addition to PRODH and P5CDH activities, some PutA proteins, such as *Escherichia coli* PutA, serve as transcriptional repressors of the *put* regulon, which includes the genes for PutA and the proline transporter PutP (Menzel & Roth, 1981*b*; Ostrovsky de Spicer & Maloy, 1993; Becker & Thomas, 2001; Wood, 1981). These 'trifunctional' PutAs contain a ribbon–helix–helix DNA-binding domain located in the N-terminal 50 residues of the polypeptide chain (Gu *et al.*, 2004). Some PutAs have biomedical importance. Most notably, recent work has shown that PutA plays a role in the virulence of *Helicobacter hepaticus*, which is closely related to the important human pathogen *H. pylori* (Krishnan *et al.*, 2008).

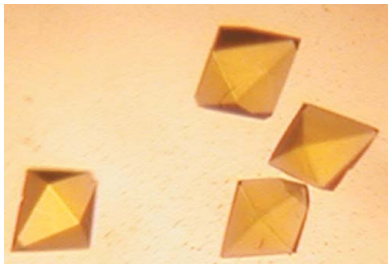

Crystal structures of PutA domains and of monofunctional PRODH and P5CDH enzymes are known, as reviewed recently (Tanner, 2008), but no structures of full-length PutAs have been reported. For example, crystal structures have been determined for the PRODH domain of *E. coli* PutA complexed with competitive inhibitors (Nadaraia *et al.*, 2001; Lee *et al.*, 2003; Zhang *et al.*, 2004) and in the dithionite-reduced state (Zhang *et al.*, 2007). The structures show that this domain features a unique $(\beta\alpha)_8$-barrel and that reduction of the cofactor induces conformational changes in the FAD ribityl chain and isoalloxazine. Crystal structures of the DNA-binding ribbon–helix–helix domain have also been determined, including a recent structure of this domain bound to DNA (Larson *et al.*, 2006; Zhou *et al.*, 2008). Furthermore, several structures are available for monofunctional *T. thermophilus* PRODH (White *et al.*, 2007, 2008) and P5CDH (Inagaki *et al.*, 2006 2007) with various ligands and cofactors bound in the active sites.

Although these structures have provided tremendous insight into the individual functions of PutA, they do not help us to understand how PutA coordinates its multiple functions. In particular, biochemical data suggest that the P5C intermediate is protected from solvent and channeled from the PRODH active site to the P5CDH active site (Surber & Maloy, 1998). Substrate channeling has been observed in other bifunctional enzymes that catalyze successive metabolic steps and it is thought that channeling affords a metabolic advantage by facilitating movement of reactive intermediates in a pathway (Miles *et al.*, 1999; Huang *et al.*, 2001).

To gain insight into the coordination of functions by PutAs, we have attempted crystallization of several PutAs. Here, we report the crystallization of full-length PutA from *Bradyrhizobium japonicum* (BjPutA).

2. Methods and results

2.1. Expression and purification

BjPutA (999 amino-acid residues; NCBI RefSeq No. NP_773901) was expressed in *E. coli* strain Rosetta(DE3)pLysS (Novagen) from the plasmid pKA8H-BjPutA (Krishnan & Becker, 2005). The expressed protein has an N-terminal 8×His tag with a TEV protease cleavage site. Rosetta cells were grown at 310 K and 250 rev min^{-1} in NZMCY medium containing chloramphenicol (34 µg ml^{-1}) and ampicillin (100 µg ml^{-1}) to a density of A_{600} = 0.6–0.8 and induced by the addition of 0.5–1.0 m*M* IPTG. Upon induction, the temperature was lowered to 295–303 K and the rotation rate was reduced to 200 rev min^{-1}. The cells were harvested after 3–4 h by centrifugation and suspended in 5%(*v*/*v*) glycerol, 20 m*M* $MgCl_2$, 300 m*M* NaCl and 20 m*M* HEPES buffer pH 8.2. The cell suspensions were flash-frozen in liquid nitrogen and stored at 253 K.

Frozen cells were thawed in the presence of five protease inhibitors: 0.001 m*M* pepstatin, 0.01 m*M* leupeptin, 0.1 m*M* *N*-*p*-tosyl-L-phenylalanine chloromethyl ketone (TPCK), 0.5 m*M* 4-(2-aminoethyl)benzenesulfonyl fluoride hydrochloride (AEBSF) and 0.005 m*M* *trans*-epoxysuccinyl-L-leucylamido(4-guanidino)butane (E-64). Cells were disrupted in a French pressure cell at 110 MPa. The cell debris and insoluble matter were removed by centrifugation at 277 K for 60 min at 35 000*g*.

The supernatant was clarified by filtering through 0.45 and 0.2 µm filters and then loaded onto an Ni–NTA column (Qiagen Superflow) equilibrated in 5%(*v*/*v*) glycerol, 20 m*M* $MgCl_2$, 300 m*M* NaCl and 20 m*M* HEPES buffer pH 8.2. The resin was washed with equilibration buffer containing 30–50 m*M* imidazole to remove contaminating proteins and BjPutA was eluted with equilibration buffer containing 250 m*M* imidazole. Fractions containing BjPutA were pooled, supplemented with FAD to a final concentration of 0.05 m*M* and dialyzed in the dark into 5%(*v*/*v*) glycerol, 0.5 m*M* EDTA, 1 m*M* DTT, 50 m*M* Tris–HCl buffer pH 7.5 (buffer *A*) in preparation for anion-exchange chromatography (5 ml HiTrapQ). The sample was loaded onto the anion-exchange column, which had been equilibrated with buffer *A*, and then eluted using a gradient of 0–0.5 *M* NaCl in buffer *A* over 20 column volumes. The pooled fractions were dialyzed in the dark into a buffer containing 50 m*M* Tris–HCl, 5%(*v*/*v*) glycerol, 50 m*M* NaCl, 0.5 m*M* EDTA, 0.5 m*M* TCEP pH 7.5 and concentrated to 8–10 mg ml^{-1} using Millipore centrifugal concentrating devices. The protein concentration was estimated using the BCA and Bradford methods (Pierce kits). Gel-filtration chromatography (Superdex 200 HR 10/30) indicated a single species of apparent molecular weight corresponding to a dimer, which is consistent with previous work on this protein (Krishnan & Becker, 2005).

As described below, removal of the N-terminal histidine tag was required in order to obtain high-quality crystals of the *C*2 form. The cleavage reaction was run immediately after the Ni–NTA step as follows. Recombinant tobacco etch virus protease (TEVP) was added to the Ni–NTA fractions at a ratio of ∼1 mg TEVP per 30–40 mg BjPutA and the mixture was incubated at 303 K for 3 h. The sample was then dialyzed against the loading buffer for the Ni–NTA step and the dialyzed sample was passed though the Ni–NTA column again. The flowthrough contained the desired protein, while uncleaved BjPutA, histidine tag and TEVP were retained in the resin. The anion-exchange step was then performed as described above. After cleavage of the tag, two extra residues remained at the N-terminus (Gly-His).

2.2. Crystallization and cryoprotection

Crystallization experiments were performed using vapor diffusion at 293 K. Initial crystallization conditions were identified using Crystal Screens 1 and 2, Wizard Screens 1 and 2 and Index Screen crystal screening kits. Diamond-shaped crystals appeared in Index Screen condition No. 90 [0.2 *M* sodium formate, 20%(*w*/*v*) PEG 3350]. Optimization trials resulted in large crystals approaching 1 mm in the longest dimension (Fig. 2*a*). The best crystals were grown in hanging drops over a reservoir containing 7%(*w*/*v*) PEG 3350, 0.1 *M* sodium formate, 0.5 m*M* TCEP and 0.1 *M* bis-tris buffer pH 6.8. Crystals were prepared for low-temperature data collection by soaking in 12%(*w*/*v*) PEG 3350, 0.1 *M* sodium formate, 0.1 *M* bis-tris

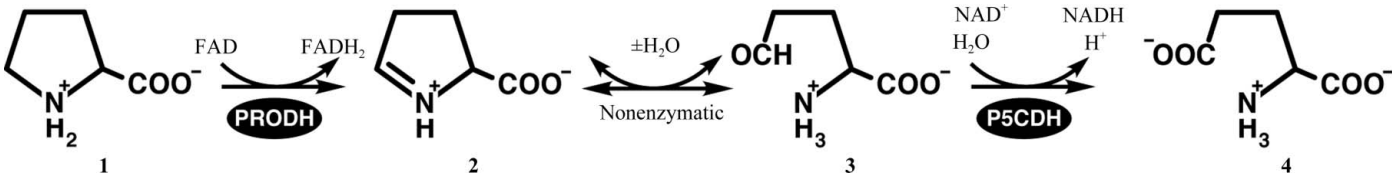

Figure 1
Reactions catalyzed by proline dehydrogenase (PRODH) and Δ^1-pyrroline-5-carboxylate dehydrogenase (P5CDH).

buffer pH 6.8, 0.25 *M* sodium ascorbate and 30%(*v*/*v*) PEG 200. The cryoprotected crystals were picked up with Hampton loops and plunged into liquid nitrogen.

While optimizing the crystallization conditions for the diamond-shaped crystals, a new crystal form with a hexagonal bipyramidal shape appeared (Fig. 2*b*). Upon optimization of this crystal form, the best specimens were grown in sitting or hanging drops using a simple reservoir solution consisting of 0.1 *M* sodium formate and 3–5%(*w*/*v*) PEG 3350. The crystals were cryoprotected by transfer to 0.15 *M* sodium formate, 15%(*w*/*v*) PEG 3350 and 40%(*v*/*v*) PEG 200 and then plunged into liquid nitrogen.

Crystal screens were also performed using protein devoid of the N-terminal histidine tag, which was removed as described in the preceding section. These screens produced crystals in the presence of a high concentration of ammonium sulfate which had the shape of rectangular blocks. Upon optimization, large crystals (~0.5–0.8 mm) were grown in sitting drops using reservoir solutions consisting of 1.7–2.1 *M* ammonium sulfate and 0.1 *M* Tris pH 7.0–8.0 (Fig. 2*c*). The crystals were cryoprotected in 2.0 *M* ammonium sulfate, 25%(*v*/*v*) glycerol and 0.1 *M* Tris pH 7.0–8.0 before plunging into liquid nitrogen. We note that this form also appeared during screening of the His-tagged enzyme, but diffraction was weak and autoindexing was problematic. Thus, removing the histidine tag appeared to improve this crystal form.

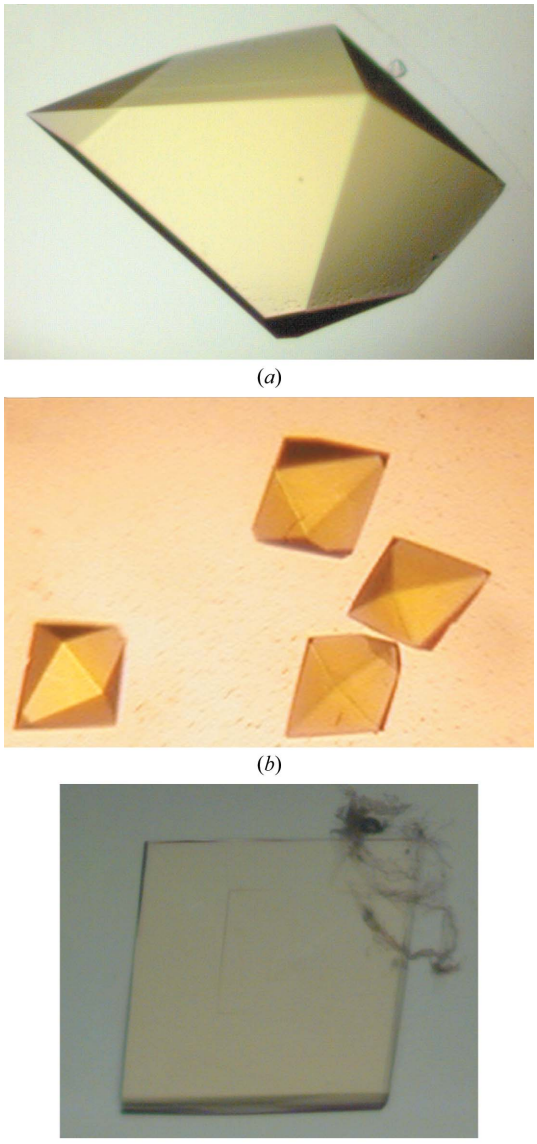

(*a*)

(*b*)

(*c*)

Figure 2
Three crystal forms of *B. japonicum* PutA: (*a*) apparent tetragonal with pseudo-merohedral twinning, (*b*) hexagonal and (*c*) centered monoclinic. The longest dimensions are approximately 0.8 mm in (*a*), 0.3 mm in (*b*) and 0.5 mm in (*c*).

Table 1
Data-processing statistics for the apparent tetragonal crystal form in various space groups.

Values in parentheses are for the outer resolution shell.

Space group	*P*422	*P*4	$P2_12_12_1$
Unit-cell parameters (Å)	*a* = 138.2, *c* = 267.3	*a* = 138.2, *c* = 267.3	*a* = 136.8, *b* = 137.4, *c* = 266.1
Resolution (Å)	46–2.70 (2.80–2.70)	46–2.70 (2.90–2.70)	46–2.70 (2.90–2.70)
Total observations	225934	225934	224652
Unique reflections	65558	117255	106445
Redundancy	3.5 (2.7)	1.9 (1.5)	2.1 (1.7)
Completeness (%)	91 (75)	86 (68)	77 (60)
Mean $I/\sigma(I)$	7.6 (2.5)	6.4 (2.0)	7.2 (2.2)
$R_{\rm merge}$†	0.114 (0.343)	0.094 (0.284)	0.089 (0.295)

† $R_{\rm merge} = \sum_{hkl}\sum_i |I_i(hkl) - \langle I(hkl)\rangle| / \sum_{hkl}\sum_i I_i(hkl)$, where $I_i(hkl)$ is the *i*th observation of reflection *hkl* and $\langle I(hkl)\rangle$ is the weighted average intensity for all observations of reflection *hkl*.

2.3. Data collection, processing and twinning assessment for the apparent tetragonal form

The diamond-shaped crystals (Fig. 2*a*) were analyzed on beamline 4.2.2 of the Advanced Light Source. Autoindexing, integration and scaling calculations were performed with *d*TREK* (Pflugrath, 1999). Autoindexing suggested a primitive tetragonal lattice with unit-cell parameters *a* = 138, *c* = 267 Å. A data set consisting of 160 frames was collected with a crystal-to-detector distance of 300 mm, a detector angle of 7°, an oscillation width of 0.5° and an exposure time of 5 s per frame.

Reasonable processing statistics could be obtained in space groups *P*422 and *P*4 (Table 1); however, the standard statistical indicators suggested a strong likelihood of twinning. For example, the average value of $\langle I^2(h)\rangle/\langle I(h)\rangle^2$ was 1.7 for acentric reflections in the resolution range 10–3.5 Å. For reference, the expected values are 2.0 and 1.5 for untwinned and perfectly twinned data, respectively (Redinbo & Yeates, 1993). Furthermore, the Padilla and Yeates local intensity difference statistic $\langle|L|\rangle$ was 0.43, which should be compared with expected values of 0.500 and 0.375 for untwinned and perfectly twinned data, respectively (Padilla & Yeates, 2003). The *L* curve for acentric data processed in space group *P*422 is shown in Fig. 3. Note that the experimental curve falls between the line that is expected for untwinned data and the concave downward curve representing perfectly twinned data. Additional analysis performed with *phenix.xtriage* (Zwart *et al.*, 2008) suggested that the data exhibit pseudo-merohedral twinning with twin operator (*k*, −*h*, *l*) and a twin fraction of approximately 0.4. In this case, the true space group is $P2_12_12_1$, with unit-cell parameters *a* = 136.8, *b* = 137.4, *c* = 266.1 Å. The assumption of four molecules in the asymmetric unit of the $P2_12_12_1$ cell results in an estimated solvent content of 57% and a $V_{\rm M}$ of 2.9 Å^3 Da^{-1} (Matthews, 1968; Kantardjieff & Rupp, 2003). Data-processing statistics for this data set merged in space group $P2_12_12_1$ are shown in Table 1.

2.4. Data collection and processing for the hexagonal crystal form

The hexagonal bipyramidal crystals (Fig. 2*b*) were analyzed on Advanced Photon Source beamline 19-BM. A 2.3 Å resolution data

Table 2
Data-processing statistics for the hexagonal crystal form.

Values in parentheses are for the outer resolution shell.

Space group	$P6_222$
Beamline	APS 19-BM
Wavelength (Å)	0.97918
Unit-cell parameters (Å)	a = 142.4, c = 181.3
Resolution (Å)	50–2.30 (2.38–2.30)
Total observations	333364
Unique reflections	47931
Redundancy	7.0 (7.1)
Completeness (%)	98.5 (99.8)
Mean $I/\sigma(I)$	21.5 (4.5)
$R_{\rm merge}$†	0.071 (0.459)

† $R_{\rm merge} = \sum_{hkl}\sum_i |I_i(hkl) - \langle I(hkl)\rangle| / \sum_{hkl}\sum_i I_i(hkl)$, where $I_i(hkl)$ is the ith observation of reflection hkl and $\langle I(hkl)\rangle$ is the weighted average intensity for all observations of reflection hkl.

set was obtained and the data were processed with *HKL*-2000 (Otwinowski & Minor, 1997). The data set consisted of 234 frames collected with an oscillation width of 0.25° per frame, an exposure time of 2.5 s per frame and a crystal-to-detector distance of 194 mm. Data-processing calculations suggested 6/*mmm* Laue symmetry with unit-cell parameters a = 142.4, c = 181.3 Å. The assumption of one BjPutA molecule per asymmetric unit leads to an estimated solvent content of 50% and a $V_{\rm M}$ of 2.4 Å^3 Da^{-1}. Data-processing statistics are shown in Table 2.

2.5. Data collection and processing for the monoclinic crystal form

The rectangular blocks grown in ammonium sulfate (Fig. 2*c*) were analyzed on ALS beamline 4.2.2. *MOSFLM* (Leslie, 2006) was used for autoindexing and integration calculations. *SCALA* (Evans, 2006) was used for scaling calculations. A 2.3 Å resolution data set consisting of 720 frames was collected with an oscillation width of 0.25° per frame, an exposure time of 5 s per frame and a crystal-to-detector distance of 160 mm. Autoindexing calculations were robust and indicated a *C*2 lattice with unit-cell parameters a = 167.0, b = 196.0, c = 108.1 Å, β = 121.6°. The assumption of two BjPutA molecules per asymmetric unit results in an estimated solvent content of 64% and a $V_{\rm M}$ of 3.5 Å^3 Da^{-1}. See Table 3 for data-processing statistics.

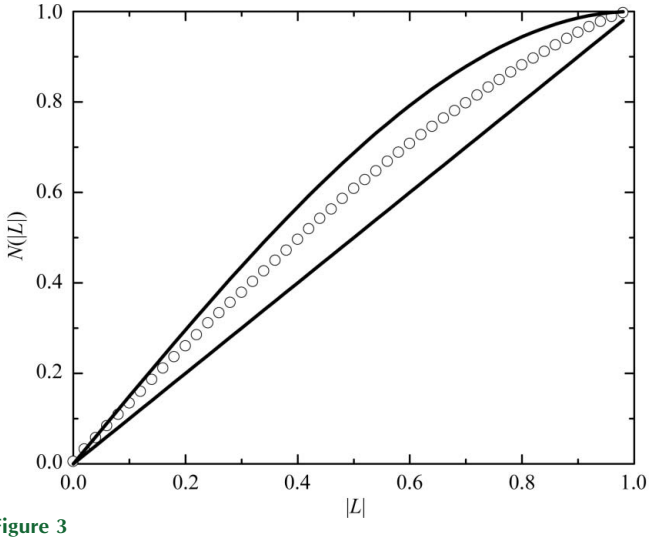

Figure 3
Analysis of local intensity differences (Padilla & Yeates, 2003) for acentric reflections collected from a diamond-shaped crystal and processed in space group *P*422. The circles represent the experimental data. The diagonal line represents the expected result for untwinned data. The upper curve represents the expected result for perfectly twinned data. Values of $N(|L|)$ were generated with *phenix.xtriage*.

Table 3
Data-processing statistics for the monoclinic crystal form.

Values in parentheses are for the outer resolution shell.

Space group	*C*2
Beamline	ALS 4.2.2
Wavelength (Å)	1.07200
Unit-cell parameters (Å, °)	a = 167.0, b = 196.0, c = 108.1, β = 121.6
Resolution (Å)	39–2.30 (2.42–2.30)
Total observations	472178
Unique reflections	130268
Redundancy	3.6 (2.9)
Completeness (%)	99.5 (96.6)
Mean $I/\sigma(I)$	9.8 (2.4)
$R_{\rm merge}$†	0.131 (0.492)

† $R_{\rm merge} = \sum_{hkl}\sum_i |I_i(hkl) - \langle I(hkl)\rangle| / \sum_{hkl}\sum_i I_i(hkl)$, where $I_i(hkl)$ is the ith observation of reflection hkl and $\langle I(hkl)\rangle$ is the weighted average intensity for all observations of reflection hkl.

The structure of BjPutA has been solved using a combination of SeMet MAD phasing and molecular replacement with the crystal forms described here. Details will be provided in a forthcoming article.

We thank Dr Jay Nix of ALS beamline 4.2.2 and Dr Stephan L. Ginell of APS SBC beamlines for assistance with data collection and processing. This research was supported by NIH grants GM065546 and GM061068. The Advanced Light Source is supported by the Director, Office of Science, Office of Basic Energy Sciences of the US Department of Energy under contract No. DE-AC02-05CH11231. The results shown in this report are derived in part from work performed at Argonne National Laboratory, Structural Biology Center at the Advanced Photon Source. Argonne is operated by UChicago Argonne LLC for the US Department of Energy, Office of Biological and Environmental Research under contract No. DE-AC02-06CH11357.

References

Adams, E. & Frank, L. (1980). *Annu. Rev. Biochem.* **49**, 1005–1061.
Becker, D. F. & Thomas, E. A. (2001). *Biochemistry*, **40**, 4714–4721.
Brown, E. D. & Wood, J. M. (1993). *J. Biol. Chem.* **268**, 8972–8979.
Evans, P. (2006). *Acta Cryst.* D**62**, 72–82.
Gu, D., Zhou, Y., Kallhoff, V., Baban, B., Tanner, J. J. & Becker, D. F. (2004). *J. Biol. Chem.* **279**, 31171–31176.
Huang, X., Holden, H. M. & Raushel, F. M. (2001). *Annu. Rev. Biochem.* **70**, 149–180.
Inagaki, E., Ohshima, N., Sakamoto, K., Babayeva, N. D., Kato, H., Yokoyama, S. & Tahirov, T. H. (2007). *Acta Cryst.* F**63**, 462–465.
Inagaki, E., Ohshima, N., Takahashi, H., Kuroishi, C., Yokoyama, S. & Tahirov, T. H. (2006). *J. Mol. Biol.* **362**, 490–501.
Kantardjieff, K. A. & Rupp, B. (2003). *Protein Sci.* **12**, 1865–1871.
Krishnan, N. & Becker, D. F. (2005). *Biochemistry*, **44**, 9130–9139.
Krishnan, N., Doster, A. R., Duhamel, G. E. & Becker, D. F. (2008). *Infect. Immun.* **76**, 3037–3044.
Larson, J. D., Jenkins, J. L., Schuermann, J. P., Zhou, Y., Becker, D. F. & Tanner, J. J. (2006). *Protein Sci.* **15**, 1–12.
Lee, Y. H., Nadaraia, S., Gu, D., Becker, D. F. & Tanner, J. J. (2003). *Nature Struct. Biol.* **10**, 109–114.
Leslie, A. G. W. (2006). *Acta Cryst.* D**62**, 48–57.
Matthews, B. W. (1968). *J. Mol. Biol.* **33**, 491–497.
Menzel, R. & Roth, J. (1981*a*). *J. Biol. Chem.* **256**, 9755–9761.
Menzel, R. & Roth, J. (1981*b*). *J. Mol. Biol.* **148**, 21–44.
Miles, E. W., Rhee, S. & Davies, D. R. (1999). *J. Biol. Chem.* **274**, 12193–12196.
Nadaraia, S., Lee, Y.-H., Becker, D. F. & Tanner, J. J. (2001). *Acta Cryst.* D**57**, 1925–1927.
Ostrovsky de Spicer, P. & Maloy, S. (1993). *Proc. Natl Acad. Sci. USA*, **90**, 4295–4298.
Otwinowski, Z. & Minor, W. (1997). *Methods Enzymol.* **276**, 307–326.
Padilla, J. E. & Yeates, T. O. (2003). *Acta Cryst.* D**59**, 1124–1130.

Pflugrath, J. W. (1999). *Acta Cryst.* D**55**, 1718–1725.
Phang, J. M. (1985). *Curr. Top. Cell. Reg.* **25**, 92–132.
Ratzkin, B. & Roth, J. (1978). *J. Bacteriol.* **133**, 744–754.
Redinbo, M. R. & Yeates, T. O. (1993). *Acta Cryst.* D**49**, 375–380.
Surber, M. W. & Maloy, S. (1998). *Arch. Biochem. Biophys.* **354**, 281–287.
Tanner, J. J. (2008). *Amino Acids*, doi:10.1007/s00726-008-0062-5.
Vinod, M. P., Bellur, P. & Becker, D. F. (2002). *Biochemistry*, **41**, 6525–6532.
White, T. A., Johnson, W. H. Jr, Whitman, C. P. & Tanner, J. J. (2008). *Biochemistry*, **47**, 5573–5580.
White, T. A., Krishnan, N., Becker, D. F. & Tanner, J. J. (2007). *J. Biol. Chem.* **282**, 14316–14327.
Wood, J. M. (1981). *J. Bacteriol.* **146**, 895–901.
Zhang, M., White, T. A., Schuermann, J. P., Baban, B. A., Becker, D. F. & Tanner, J. J. (2004). *Biochemistry*, **43**, 12539–12548.
Zhang, W., Zhang, M., Zhu, W., Zhou, Y., Wanduragala, S., Rewinkel, D., Tanner, J. J. & Becker, D. F. (2007). *Biochemistry*, **46**, 483–491.
Zhou, Y., Larson, J. D., Bottoms, C. A., Arturo, E. C., Henzl, M. T., Jenkins, J. L., Nix, J. C., Becker, D. F. & Tanner, J. J. (2008). *J. Mol. Biol.* **381**, 174–188.
Zhu, W. & Becker, D. F. (2003). *Biochemistry*, **42**, 5469–5477.
Zwart, P. H., Afonine, P. V., Grosse-Kunstleve, R. W., Hung, L. W., Ioerger, T. R., McCoy, A. J., McKee, E., Moriarty, N. W., Read, R. J., Sacchettini, J. C., Sauter, N. K., Storoni, L. C., Terwilliger, T. C. & Adams, P. D. (2008). *Methods Mol. Biol.* **426**, 419–435.